Spin-Light Coherence for Single-Spin Measurement and Control in Diamond

B. B. Buckley, *et al.*

Science **330**, 1212 (2010);
DOI: 10.1126/science.1196436

G. V. Bicknell, Eds. (ASP Conference Series Vol. 121, Astronomical Society of the Pacific, San Francisco, 1997), pp. 845–866.
9. R. E. Pudritz, R. Ouyed, Ch. Fendt, A. Brandenburg, in *Protostars and Planets V*, B. Reipurth, D. Jewitt, K. Keil, Eds. (University of Arizona Press, Tucson, AZ, 2007), pp. 277–294.
10. A. Chrysostomou, P. W. Lucas, J. H. Hough, *Nature* **450**, 71 (2007).
11. J. A. Morse, S. Heathcote, G. Cecil, P. Hartigan, J. C. Raymond, *Astrophys. J.* **410**, 764 (1993).
12. A. H. Bridle, R. A. Perley, *Annu. Rev. Astron. Astrophys.* **22**, 319 (1984).
13. I. F. Mirabel, L. F. Rodríguez, *Annu. Rev. Astron. Astrophys.* **37**, 409 (1999).
14. J. Martí, L. F. Rodríguez, B. Reipurth, *Astrophys. J.* **449**, 184 (1995).
15. G. Pech *et al.*, *Astrophys. J.* **712**, 1403 (2010).
16. L. F. Rodríguez *et al.*, *Astrophys. J.* **346**, L85 (1989).
17. J. Martí, L. F. Rodríguez, B. Reipurth, *Astrophys. J.* **416**, 208 (1993).
18. G. Garay, S. Ramirez, L. F. Rodriguez, S. Curiel, J. M. Torrelles, *Astrophys. J.* **459**, 193 (1996).
19. D. J. Wilner, M. J. Reid, K. M. Menten, *Astrophys. J.* **513**, 775 (1999).
20. J. M. Girart, S. Curiel, L. F. Rodríguez, J. Cantó, *Rev. Mex. Astron. Astrofis.* **38**, 169 (2002).
21. L. F. Rodríguez, G. Garay, K. Brooks, D. Mardones, *Astrophys. J.* **626**, 953 (2005).
22. Circularly polarized emission has been reported in the ejecta of the young star T Tauri South (*41*), but in this case the proposed mechanism is gyrosynchrotron, which has different polarization characteristics than synchrotron and is expected to be relevant only close to the stellar surfaces.
23. A. R. Bell, *Mon. Not. R. Astron. Soc.* **182**, 147 (1978).
24. See supporting material on *Science* Online.
25. G. Schaller, D. Schaerer, G. Meynet, A. Maeder, *Astron. Astrophys. Suppl. Ser.* **96**, 269 (1992).
26. L. F. Rodríguez, J. M. Moran, P. T. P. Ho, E. W. Gottlieb, *Astrophys. J.* **235**, 845 (1980).
27. M. Lyutikov, V. I. Pariev, D. C. Gabuzda, *Mon. Not. R. Astron. Soc.* **360**, 869 (2005).
28. A. G. Pacholczyk, *Radio Astrophysics* (Freeman, San Francisco, 1970).
29. R. Beck, M. Krause, *Astron. Nachr.* **326**, 414 (2005).
30. R. L. Curran, A. Chrysostomou, *Mon. Not. R. Astron. Soc.* **382**, 699 (2007).
31. J. L. Gómez, A. P. Marscher, S. G. Jorstad, I. Agudo, M. Roca-Sogorb, *Astrophys. J.* **681**, L69 (2008).
32. S. Cabrit, *Int. Astron. Union Symp.* **243**, 203 (2007).
33. S. Lizano, F. H. Shu, D. Galli, A. Glassgold, *Rev. Mex. Astron. Astrof. Ser. Conf.* **36**, 149 (2009).
34. T. P. Ray, *Rev. Mex. Astron. Astrof. Ser. Conf.* **36**, 179 (2009).
35. E. M. de Gouveia dal Pino, *AIP Conf. Proc.* **784**, 183 (2005).
36. B. Reipurth, J. Bally, *Annu. Rev. Astron. Astrophys.* **39**, 403 (2001).
37. W. H. T. Vlemmings, G. Surcis, K. J. E. Torstensson, H. J. van Langevelde, *Mon. Not. R. Astron. Soc.* **404**, 134 (2010).
38. J. M. Girart, R. Rao, D. P. Marrone, *Science* **313**, 812 (2006).
39. V. Bosch-Ramon, G. E. Romero, A. T. Araudo, J. M. Paredes, *Astron. Astrophys.* **511**, A8 (2010).
40. N. A. Patel *et al.*, *Nature* **437**, 109 (2005).
41. T. P. Ray *et al.*, *Nature* **385**, 415 (1997).

42. National Radio Astronomy Observatory is a facility of the NSF, operated under cooperative agreement by Associated Universities, Incorporated. We acknowledge I. Agudo, A. Alberdi, and J. L. Gómez for useful comments. G.A., C.C.-G., J.M., M.O., and J.M.T. acknowledge support from Ministerio de Ciencia e Innovación (Spain) grants AYA2008-06189-C03 and AYA2007-68034-C03-02 [co-funded with Fondo Europeo de Desarrollo Regional (FEDER) funds] and from Junta de Andalucía (Spain). L.F.R. acknowledges the support of Dirección General de Asuntos del Personal Académico, UNAM, and Consejo Nacional de Ciencia y Tecnología, México.

Supporting Online Material

www.sciencemag.org/cgi/content/full/330/6008/1209/DC1
Materials and Methods
SOM Text
Table S1
References

26 July 2010; accepted 20 October 2010
10.1126/science.1195589

Spin-Light Coherence for Single-Spin Measurement and Control in Diamond

B. B. Buckley, G. D. Fuchs, L. C. Bassett, D. D. Awschalom*

The exceptional spin coherence of nitrogen-vacancy centers in diamond motivates their function in emerging quantum technologies. Traditionally, the spin state of individual centers is measured optically and destructively. We demonstrate dispersive, single-spin coupling to light for both nondestructive spin measurement, through the Faraday effect, and coherent spin manipulation, through the optical Stark effect. These interactions can enable the coherent exchange of quantum information between single nitrogen-vacancy spins and light, facilitating coherent measurement, control, and entanglement that is scalable over large distances.

The coherent coupling of light with matter provides a powerful tool for quantum measurement and control. The resulting hybrid states have been employed in individually addressable semiconducting (*1*), atomic (*2*), and superconducting (*3*) quantum systems. Individual diamond nitrogen-vacancy (NV) centers (*4*) show great promise as solid-state spin qubits with demonstrations of millisecond coherence times (*5*) and nanosecond manipulation times (*6*). NV-center spins coherently couple to nearby electronic (*7*, *8*) and nuclear (*9*, *10*) spins, creating few-qubit networks for simple algorithms and quantum memories. NV-center spin states are conventionally read out destructively with the use of spin-dependent photoluminescence (PL). We present nondestructive single-spin measurement via the Faraday effect (FE) and unitary single-spin manipulation via the optical Stark effect (OSE) with the use of a near-resonant laser field coupled to an NV center. With enhanced coupling from an optical cavity, these techniques can be extended to quantum weak and quantum nondemolition measurements of single spins, facilitating applications such as quantum repeaters (*11*) and spin-photon entanglement (*12*) on demand. This approach may also assist with the study of newly identified defect-based spin systems (*13*) with limited single-spin read-out alternatives.

The FE and OSE probe the respective light and spin responses to the near-resonant coupling between an NV center and light, which emerge from spin-dependent optical transitions (*14*). Each optical transition's ground ($|g\rangle$) and excited ($|e\rangle$) states coherently mix with the laser field (Fig. 1A), forming polariton states ($|G\rangle$ and $|E\rangle$) whose energies repel in the form of a level anticrossing (Fig. 1A, inset) as a function of the energy detuning (Δ) between the light and the optical transition. The groundlike polariton states ($|G\rangle$) adiabatically remain occupied as they shift in energy during the interaction. The FE originates from polarization selection rules in which the coupled polarization component of the coherent optical field experiences a spin-dependent phase shift relative to the other. Simultaneously, the OSE energy shifts add quantum phases to the spin states producing spin rotation. Theoretical predictions of the FE and OSE from a modified Jaynes-Cummings model are in quantitative agreement with our measurements (*15*).

A diamond NV center consists of a vacancy adjacent to a substitutional nitrogen atom in the diamond lattice. When negatively charged, the orbital ground state is a spin triplet whose levels function as a qubit (*4*) and are tunable with an applied magnetic field. Microwave magnetic fields that are resonant and near-resonant (*16*) with the spin transitions produce unitary rotations of the spin state. NV centers exhibit spin-conserving optical transitions (Fig. 1B) to an orbital-doublet, spin-triplet excited state 1.945 eV above the ground state (*17*). An NV center may be optically excited into the excited state, either resonantly at 637 nm or with higher-energy light along with phonon creation. Phonons can also be created during spontaneous emission back to the ground state, resulting in red-shifted PL. Optical excitation causes spin polarization from the $m_s = \pm 1$ spin states into the $m_s = 0$ spin state through an intersystem-crossing decay mechanism. PL is inhibited during the 460-ns cryogenic lifetime (*18*) of this decay, resulting in a spin-dependent PL intensity that is used for destructive spin-projection measurements. These dynamics allow individual NV centers to be optically addressed.

The NV-center spin coherently couples to light in our measurements because the optical transition energies (Fig. 1C) vary by spin state as a result of spin-spin and spin-orbit interactions (*19*). These transitions are energetically stable

Center for Spintronics and Quantum Computation, University of California, Santa Barbara, CA 93106, USA.

*To whom correspondence should be addressed. E-mail: awsch@physics.ucsb.edu

(*20*) in pure diamond hosts under cryogenic temperatures (*21*). In our NV centers, the transverse crystal strain is strong enough to energetically separate the excited-state orbital doublet into two branches with approximately linear, orthogonal optical-transition dipoles aligned to the transverse strain: ^3E_X and ^3E_Y (*22*). These dipoles couple to orthogonal near-linear polarizations of light, giving rise to the FE in a nonstandard polarization basis. A magnetic field is applied along the NV symmetry axis to produce similar spin eigenstates in both the ground and excited orbitals, providing robust spin-conserving optical transitions. In the range of crystal strains and magnetic fields that we studied, the largest optical transition–energy spin splitting occurs in the lower-energy excited-state orbital branch (^3E_Y). The ^3E_Y, m_s = –1 optical transition is roughly 3 GHz lower in energy than the ^3E_Y, m_s = 0 optical transition (Fig. 1C, right). The fine structure of the higher-energy excited state orbital branch (^3E_X) more closely resembles the ground-state fine structure for our experimental conditions, producing spin-conserving optical transitions that are closely spaced in energy. The spin splitting in the ^3E_Y branch is insensitive to changes in strain and magnetic field when these effects dominate spin-orbit interactions, allowing the spin-light interactions investigated here to persist across a broad range of experimental conditions.

We assembled a confocal microscope to study single NV centers at cryogenic temperatures. The NV centers were naturally formed in high-purity diamond grown by chemical vapor deposition specified to contain less than 5 parts per billion nitrogen impurities. A 0.85–numerical aperture microscope objective focused both a red laser, tunable in energy across the NV-center optical transitions at 637 nm, and a green 532-nm laser onto a single NV center for both resonant and nonresonant optical excitation, respectively. PL from the NV center's phonon sideband was collected with the objective and detected with an avalanche photodiode (APD). The PL provided two important measurements: (i) the spin projection ($\langle S_Z \rangle$) under green illumination and (ii) resonant optical absorption from photoluminescence excitation (I_{PLE}) under tunable red excitation. We used a lithographically patterned, short-terminated coplanar waveguide (*6*) to apply microwave-frequency magnetic fields for resonant spin manipulation of the ground-state triplet. The lasers, microwave fields, and measurements of PL were all gated for time-domain measurements. The polarization of the tunable red laser light was prepared relative to the orthogonal optical dipoles of the NV center, ensuring that each dipole interacted with half of the light for polarization-interference measurements. The transmitted red laser light was collected through a back-side window in the cryostat, passed through polarization optics to project the correct polarization, and then analyzed with a near shot-noise–limited balanced photodiode bridge whose signal was measured with a lock-in amplifier (*15*).

We studied the FE spin dependence and the corresponding NV-center response to a 1-μs pulse of tunable red laser light as a function of the light's energy. In the measurement sequence (Fig. 2A), the initial spin state was prepared alternately in either m_s = 0 or m_s = –1 before the red laser light pulse. The measured spin-dependent FE (Φ_F) is the difference in phase shift of the red laser light polarization between the two spin preparations. Additionally, both I_{PLE} and $\langle S_Z \rangle$ were measured for both prepared spin states with PL measured at different times during the sequence. To increase the signal-to-noise ratio, Φ_F, I_{PLE}, and $\langle S_Z \rangle$ data were averaged for ~5 × 10^6 repeated measurements, requiring ~30 s per point. These three independent measurements were correlated as the red laser light energy was tuned across the optical transitions, providing a detailed picture of the full interaction dynamics.

To illustrate the FE dynamics in our system, simultaneous measurements of Φ_F, I_{PLE}, and $\langle S_Z \rangle$ at a temperature of 8 K and an applied magnetic field of 1620 G are shown for the lower-energy E_Y orbital-branch optical transitions at red laser powers of 5 and 0.1 μW (Fig. 2, B and C, respectively). The E_Y, m_s = 0 optical transition (circled in Fig. 1C) defines the origin of the red laser energy scale, placing the E_Y, m_s = –1 optical transition near –3-GHz laser energy in all presented FE data. As a result of spectral broadening of the optical transitions (*21*), Φ_F is also broadened, resulting in a reduced response near resonances. The m_s = ±1 spin states are susceptible to polarization into the m_s = 0 spin state when optically excited because of the intersystem-crossing decay, which is measured directly with $\langle S_Z \rangle$. Therefore, optical spin polarization reduces Φ_F and I_{PLE} signals more substantially near resonance with m_s = ±1 optical transitions and at higher powers. Photo-ionization (*23*) may also result from red laser excitation, which reduces Φ_F and I_{PLE} signals and skews $\langle S_Z \rangle$. The NV center is less perturbed at lower red laser powers, producing more symmetric FE data at smaller signal intensities (Fig. 2C). The temperature dependence of the FE that we measured (*15*) was consistent with previous studies of the excited-state energetic stability with temperature (*21*). Using our developed model (*15*) along with our measured FE response, we determined that the average, equal-intensity area of the red laser confocal spot was (0.75 ± 0.1 μm)^2, which is consistent with diffraction, drift, and aberration limits.

FE measurements showing both E_X and E_Y orbital-branch optical transitions at a temperature of 8 K, an applied magnetic field of 1920 G, and a higher red laser power of 15 μW are shown in Fig. 2D. The m_s = 0 and m_s = –1 optical transitions in the E_X orbital branch (near 16.5-GHz laser energy) are closer together in energy than

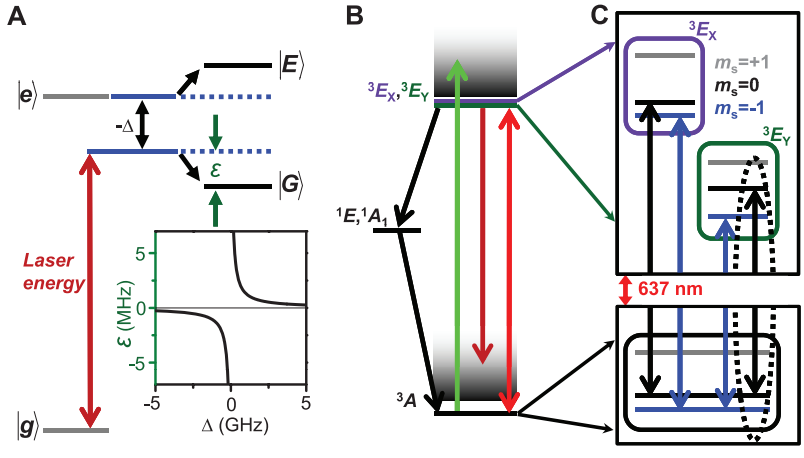

Fig. 1. (**A**) An optical transition interacting with a laser detuned in energy by Δ relative to the transition energy. Under adiabatic conditions, the spin-light polariton energy levels shift by ε as a result of the interaction, producing measurable effects in both the phase of interacting light and the NV-center spin dynamics. (Inset) ε as a function of Δ. (**B**) NV-center energy-level diagram depicting ground (^3A) and excited (^3E_X, ^3E_Y) spin triplet levels. From left to right: Diagonal arrows show the intersystem crossing from the excited m_s = ±1 states to the ground m_s = 0 state through singlet-level (^1E, $^1A_1$) metastable decay, which permits spin initialization and measurement. The nonresonant green upward and red downward arrows depict optical excitation and collected PL, respectively. The red double arrow depicts the multiple resonant transitions magnified in (C). (**C**) Fine structure of the presented NV-center ground- and excited-state energy levels at 1920 G, additionally depicting spin-conserving optical transitions for m_s = 0 (black arrows) and m_s = –1 (blue arrows) spin states in both excited-state orbitals. The E_Y, m_s = 0 (circled) spin-conserving transition is ~3 GHz larger in energy than the E_Y, m_s = –1 transition for our measurements. With increased strain, ^3E_X and ^3E_Y orbital energies further separate. An increase in magnetic field shifts the m_s = +1 and m_s = –1 spin sublevels up and down, respectively, in all orbital branches, having only an indirect effect on changing spin-conserving optical transition energies.

their spectrally broadened absorption and spin polarization widths, making them difficult to differentiate and reducing Φ_F for this orbital branch. Optical coupling to the E_X orbital branch is 40% weaker relative to the E_Y orbital branch due to the NV center's orientation, further reducing Φ_F for the E_X orbital branch. The E_X orbital branch picks up a stronger $m_s = 0$ optical transition response in Φ_F, probably because the $m_s = -1$ spin decays more easily through the intersystem crossing, which inhibits the FE during its lifetime. Data from the E_Y orbital-branch optical transitions in Fig. 2D resemble those of Fig. 2, B and C, but at a higher power, showing an increased asymmetry between the $m_s = 0$ and $m_s = -1$ optical transitions. Optical transitions that do not conserve the spin state can also be observed at this red laser power. Black arrows between I_{PLE} and $\langle S_Z \rangle$ graphs denote the four spin-conserving transition energies, with the E_X transitions being nearly degenerate. Blue and red arrows denote the expected positions of spin-nonconserving transitions coupled to the $m_s = 0$ and $m_s = -1$ ground spin states, respectively. Sharp features in both I_{PLE} and $\langle S_Z \rangle$ are consistent with these spin-nonconserving optical transition energies but do not line up exactly with their expected positions because the hysteretic and nonlinear response of the red laser energy tuning was not actively corrected. FE measurements on a different NV center gave nearly identical results for both E_X and E_Y orbital branches, although these orbital transitions were further separated in energy as a result of higher crystal strain.

Complementary to the light's FE response, the NV-center spin also coherently reacts to its dispersive interactions with light in the form of the OSE. The OSE manifests as relative energy shifts of the ground spin eigenstates, which alter the spin's Larmor precession rate during interaction with the red laser light pulse. This process is equivalent to a σ_Z spin rotation of the spin qubit in the Bloch sphere rotating frame representation. We measured the OSE with the use of a modified Hahn echo microwave pulse sequence (Fig. 3A) to mitigate slow environmental dephasing. The red laser interaction was timed between the two final Hahn microwave pulses such that the OSE spin evolution is encoded in the final spin state that was measured with PL intensity (I_{PL}). Through phase control of the final Hahn echo pulse, we measured multiple spin projections to give a more detailed picture of the OSE spin dynamics. Figure 3B shows the OSE spin rotation as a function of red laser pulse duration. All OSE spin projection data were averaged over 2.5×10^5 repeated measurements, taking 2.6 s for each data point and ~15 min for typical scans. An exponentially decaying sinusoidal fit to these data determines the Larmor frequency shift (Σ_S) induced by the OSE for fixed red laser energy and power. When the laser detuning is much larger than the resonant optical Rabi frequency, Σ_S is nearly linear with laser power (Fig. 3C). We determined the ground-state spin coherence to be

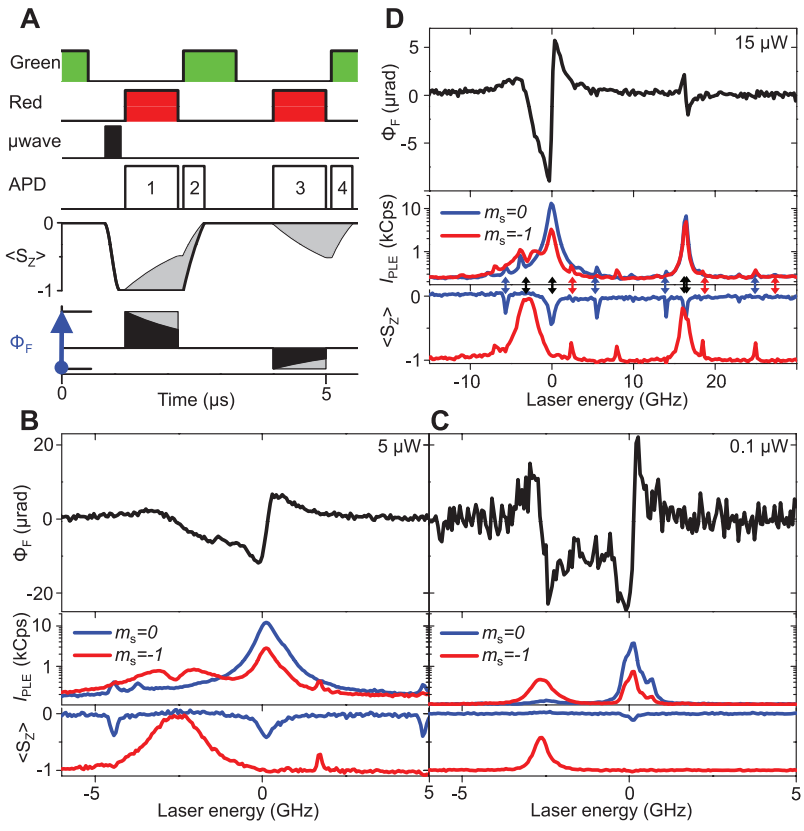

Fig. 2. (**A**) FE measurement timing sequence showing the gated green laser, tunable red laser, microwave, and multiplexed APD timing, as well as the spin-state evolution and diode bridge signal in time. PL photons are binned separately in time to measure both I_{PLE} (APD bins 1, 3) and $\langle S_Z \rangle$ (APD bins 2,4) for the $m_s = -1$ and $m_s = 0$ prepared spin states. Gray areas indicate possible spin-polarization effects from the red laser. Φ_F (denoted by the blue arrow at bottom-left) is the difference in measured red laser polarization response between the prepared $m_s = 0$ and $m_s = -1$ spin states. (**B** and **C**) FE data sets scaled identically showing Φ_F, as well as I_{PLE} and $\langle S_Z \rangle$, for both $m_s = 0$ (blue) and $m_s = -1$ (red) prepared spin states of the ^3E_Y orbital-branch optical transitions at 5 and 0.1 μW red laser power, respectively. The $m_s = 0$ optical transition (at 0-GHz laser energy) is more robust against spin polarization than the $m_s = -1$ optical transition (near −3-GHz laser energy). μrad, microradians; kCps, photon kilocounts per second. (**D**) FE data set at 15 μW scanning across both ^3E_X and ^3E_Y orbital-branch optical transition energies. The measured FE is substantially reduced for the ^3E_X orbital transitions (near 16.5 GHz), primarily as a result of the smaller optical transition energy splitting between the spin states. Vertical-pointing double arrows denote expected transition energies, as described in the text.

$T_2 = 480$ μs with Gaussian decay using a Hahn echo sequence without applying the OSE, revealing that pure spin decoherence is a negligible effect in the OSE data.

By comparing the FE and OSE responses together as a function of red laser energy, we analyzed both light and spin components of the polariton dynamics, which gives deeper insight into the full NV-center spin interactions with coherent light. Φ_F and Σ_S data are superimposed as a function of laser energy at a temperature of 8 K, an applied magnetic field of 1920 G, and a red laser power of 0.66 μW (Fig. 3D, top). By fitting Σ_S as a function of laser energy, the resonant optical Rabi frequency was indirectly determined to be $2\pi \times 70$ MHz at this laser power. The relation between Φ_F and Σ_S gives information regarding the mean photon number of the interaction (*15*), which can be used to calibrate the response to stronger light coupling, down to the single-photon level.

The decay of the OSE oscillations present in Fig. 3B can be analyzed in terms of dephasing between the repeated interrogations of the OSE-shifted spin. The number of OSE oscillations to $1/e$ exponential decay (N_D) in Fig. 3E is plotted as a function of laser energy for two laser powers. The smallest number of coherent oscillations occurs near the optical resonances where absorption, spin polarization (Fig. 3D, bottom), and spectral diffusion become most prominent. Although there are probably several sources of fundamental decoherence and experimental dephasing, these data qualitatively agree with the red line in Fig. 3E, which is a fit using a model that includes only two contributions (*15*): first, dephasing from spectral hopping giving a distribution of transition energies, and second, dephasing from the red laser

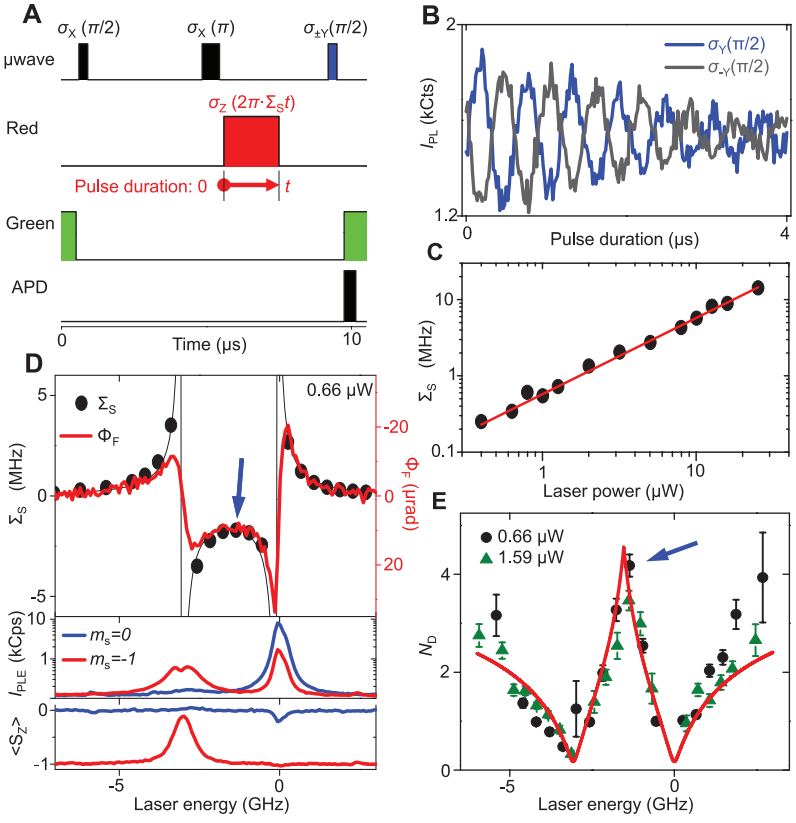

Fig. 3. (**A**) OSE measurement timing sequence. The red laser produces a σ_Z spin rotation proportional to its 0- to 4-μs pulse duration. $\langle S_Z \rangle$ follows $\pm\sin(\sigma_Z)$ as a result of a ±90° microwave phase shift of the final Hahn echo pulse. (**B**) I_{PL} of sequences that have these two microwave phases. kCts, photon kilocounts. (**C**) Σ_S as a function of laser power at ~2-GHz laser energy. The error is represented by the data-point size and is dominated by the 15% uncertainty in the laser power calibration. The red line is a linear fit of Σ_S with 5.74 MHz per microwatt slope. (**D**) Comparison of Σ_S and Φ_F showing their complimentary response as a function of laser energy and also showing I_{PLE} and $\langle S_Z \rangle$ taken with Φ_F for both prepared spin states. OSE and FE data sets were taken under the same experimental conditions at 0.66-μW laser power. The Σ_S data point denoted by the blue arrow is the frequency fit of the data presented in Fig. 3B. (**E**) OSE spin coherence measured in number (N_D) of σ_Z rotations to the 1/*e* decay point. Black circles represent the measurements with 0.66-μW red laser power (Fig. 3D), and green triangles represent measurements with 1.59-μW red laser power. The blue arrow denotes the N_D data point fit from in Fig. 3B. The red line is a fit to the data using a model incorporating dephasing from spectral broadening and laser intensity fluctuations. Error bars indicate standard errors of OSE data fits.

intensity fluctuations. The fit yields a spectral hopping half width at half maximum of 63 ± 13 MHz and laser power fluctuations of 3.5 ± 0.8%. These values, along with the 71-MHz power-broadened natural linewidth, are consistent with the 150-MHz I_{PLE}-measured linewidth of the $m_s = 0$ optical transition shown in Fig. 3D. This suggests that spectral diffusion and local laser intensity fluctuations play primary roles in the decay of the OSE oscillations, consistent with recent studies of optical Rabi oscillations (*24*). The cumulative fidelity for a π spin rotation in Fig. 3B is 89 ± 1% with resistance to back-action spin flips of 98.9 ± 0.3% (*15*). These two fidelities set limits on the expected fidelity of either single-spin/single-photon entanglement generation or quantum nondemolition measurements, given an appropriately designed cavity to enhance the per-photon spin-light interaction under otherwise similar conditions. Improvements in the experimental design and material quality may mitigate the external sources of dephasing and lead to even higher-fidelity spin-light coupling for future applications of NV centers in diamond.

The coherent coupling between an NV-center spin and light is a critical advancement for the use of NV centers in quantum information science. For example, by mixing the spin eigenstates in either the ground or excited orbitals to form a V (*25*) or Λ (*26*, *27*) configuration, respectively, all-optical spin manipulation and measurement could be performed in other spin bases to span the full Bloch sphere. With the increased coupling offered by photonic cavities (*28*), these techniques enable optical quantum nondemolition measurements (*29*) of single electron spins for fundamental studies of light-matter interactions, potentially leading to solid-state implementations of quantum key distribution (*30*). Furthermore, these hybrid light-spin states could controllably couple distant NV-center spins through photonic networks (*31*) for increasingly complex quantum information processing operations.

References and Notes

1. J. Berezovsky, M. H. Mikkelsen, N. G. Stoltz, L. A. Coldren, D. D. Awschalom, *Science* **320**, 349 (2008).
2. S. A. Aljunid *et al.*, *Phys. Rev. Lett.* **103**, 153601 (2009).
3. A. Lupaşcu *et al.*, *Nat. Phys.* **3**, 119 (2007).
4. F. Jelezko, T. Gaebel, I. Popa, A. Gruber, J. Wrachtrup, *Phys. Rev. Lett.* **92**, 076401 (2004).
5. G. Balasubramanian *et al.*, *Nat. Mater.* **8**, 383 (2009).
6. G. D. Fuchs, V. V. Dobrovitski, D. M. Toyli, F. J. Heremans, D. D. Awschalom, *Science* **326**, 1520 (2009); 10.1126/science.1181193.
7. R. Hanson, V. V. Dobrovitski, A. E. Feiguin, O. Gywat, D. D. Awschalom, *Science* **320**, 352 (2008); 10.1126.1155400.
8. P. Neumann *et al.*, *Nat. Phys.* **6**, 249 (2010).
9. L. Childress *et al.*, *Science* **314**, 281 (2006); 10.1126/science.1131871.
10. P. Neumann *et al.*, *Science* **329**, 542 (2010); 10.1126/science.1189075.
11. L. Childress, J. M. Taylor, A. S. Sørensen, M. D. Lukin, *Phys. Rev. Lett.* **96**, 070504 (2006).
12. E. Togan *et al.*, *Nature* **466**, 730 (2010).
13. J. R. Weber *et al.*, *Proc. Natl. Acad. Sci. U.S.A.* **107**, 8513 (2010).
14. C. Cohen-Tannoudji, S. Reynaud, *J. Phys. B* **10**, 345 (1977).
15. Materials and methods and theoretical analysis are available as supporting material on *Science* Online.
16. C. Wei, N. B. Manson, J. P. D. Martin, *Phys. Rev. Lett.* **74**, 1083 (1995).
17. N. B. Manson, J. P. Harrison, M. J. Sellars, *Phys. Rev. B* **74**, 104303 (2006).
18. V. M. Acosta, A. Jarmola, E. Bauch, D. Budker, preprint available at http://arxiv.org/abs/1009.0032v2.
19. A. Batalov *et al.*, *Phys. Rev. Lett.* **102**, 195506 (2009).
20. P. Tamarat *et al.*, *Phys. Rev. Lett.* **97**, 083002 (2006).
21. K.-M. C. Fu *et al.*, *Phys. Rev. Lett.* **103**, 256404 (2009).
22. F. Kaiser *et al.*, preprint available at http://arxiv.org/abs/0906.3426v1.
23. N. B. Manson, J. P. Harrison, *Diamond Relat. Mater.* **14**, 1705 (2005).
24. L. Robledo, H. Bernien, I. v. Weperen, R. Hanson, *Phys. Rev. Lett.* **105**, 117403 (2010).
25. H. Kosaka *et al.*, *Nature* **457**, 702 (2009).
26. C. Santori *et al.*, *Opt. Express* **14**, 7986 (2006).
27. P. Tamarat *et al.*, *N. J. Phys.* **10**, 045004 (2008).
28. P. E. Barclay, K.-M. Fu, C. Santori, R. G. Beausoleil, *Opt. Express* **17**, 9588 (2009).
29. P. Grangier, J. A. Levenson, J.-P. Poizat, *Nature* **396**, 537 (1998).
30. J.-J. Chen, J.-H. An, M. Feng, G. Liu, *J. Phys. At. Mol. Opt. Phys.* **43**, 095505 (2010).
31. A. Imamoglu *et al.*, *Phys. Rev. Lett.* **83**, 4204 (1999).

32. We sincerely thank D. M. Toyli, C. G. Yale, F. J. Heremans, and C. Santori for thoughtful comments. We gratefully acknowledge support from the Air Force Office of Scientific Research, the Army Research Office, and Defense Advanced Research Projects Agency.

Supporting Online Material

www.sciencemag.org/cgi/content/full/science.1196436/DC1
Materials and Methods
SOM Text
Figs. S1 to S5
References

12 August 2010; accepted 5 October 2010
Published online 14 October 2010;
10.1126/science.1196436